Original Article

# Dose Shadowing and Prosthesis Involvement for Megavoltage Photon *In vivo* Diode Dosimetry

**Nicholas Ade, Dete Van Eeden, F. C. P. Du Plessis**

Department of Medical Physics, University of the Free State, Bloemfontein, South Africa

## Abstract

**Aim:** The aim of the study is to investigate the photon beam perturbations induced by an *in vivo* diode in combination with prosthesis involvement in a human-like phantom. **Materials and Methods:** Beam perturbations for 6 MV and 10 MV photons caused by an EDP-20$^{3G}$ *in vivo* diode in combination with prosthesis involvement were studied in a unique water-equivalent pelvic phantom, equipped with bony structures and Ti prosthesis using single fields between 2 × 2 and 15 cm × 15 cm as well as 10 MV lateral opposing fields and a four-field plan. Dose distributions were measured with Gafchromic EBT3 films with and without the diode included in the beams on the prosthesis (prosthetic fields) and non-prosthesis (non-prosthetic fields) sides of the phantom. Differences between prosthetic and non-prosthetic field dose data were determined to assess the effect of the prosthesis on the diode-induced beam perturbations inside the phantom. **Results:** Photon beam dose perturbations ranged from 2% to 7% and from 5% to 12% for prosthetic and non-prosthetic fields, respectively, with relative differences between 2% and 4%. In addition, $d_{50}$ depths ranging from 8.7 to 11.5 cm and from 11.5 to 15 cm were acquired in the phantom for prosthetic and non-prosthetic fields, respectively, with relative differences between 2% and 5%. **Conclusion:** On the basis of accuracy requirements in radiotherapy noting that a small underdose to tumors could yield a decrease in the probability of tumor control, the diode-induced beam perturbations in combination with prosthesis involvement in the photon fields may affect treatment outcome, as there would be a reduction in the prescribed target dose during treatment delivery.

**Keywords:** Beam perturbations, *in vivo* diode, pelvic phantom, photons, prosthesis

**Received on:** 28-06-2019 **Review completed on:** 14-09-2019 **Accepted on:** 08-10-2019 **Published on:** 11-12-2019

## Introduction

Radiation therapy (RT) is an indispensable therapeutic approach in the treatment of most malignant lesions. In RT, dosimetric differences or errors between the planned and delivered radiation doses may have an impact on the intended clinical outcome. Each of the several steps involved in the radiotherapy process may introduce an uncertainty.[1] Accurate dose delivery and techniques to monitor patient radiation doses are, therefore, a necessity for good treatment outcome.[2-5] An independent and straightforward method to verify or monitor the actual radiation dose given to patients treated with RT is by means of *in vivo* dosimetry (IVD).[2-12] For IVD, solid-state detectors are used due to their high sensitivity and high spatial resolution when compared to air-filled ionization chambers. *In vivo* measurements during a few treatment sessions are recommended for some patient groups where a high accuracy in dose delivery is required. These include three-dimensional (3D) conformal RT, intensity-modulated RT (IMRT), or in dose escalation studies.[13] Although silicon (Si) diodes can perform real-time dose measurements, point dose *in vivo* dosimetry (IVD) with diodes is not suitable for verifying IMRT and arc therapy treatments. Electronic portal imaging device (EPID) dosimetry would be most suited and is currently being developed as a future standard.[14] The present challenges of EPID-based dosimetry compared to *in vivo* diodes are that commercial solutions are not widely available due to limited availability of dedicated software and additional work is required, e.g., increased time to investigate out of tolerance results.[14,15] As a result, *in vivo* diodes are likely to remain the mainstay for simple palliative care treatments.[14]

Access this article online

Quick Response Code:

Website: www.jmp.org.in

DOI: 10.4103/jmp.JMP_59_19

**Address for correspondence:** Dr. Nicholas Ade, Department of Medical Physics, University of the Free State, PO Box 339, Bloemfontein 9300, South Africa.
E-mail: nickade00@yahoo.com



**How to cite this article:** Ade N, Eeden DV, Du Plessis FC. Dose shadowing and prosthesis involvement for megavoltage photon *In vivo* diode dosimetry. J Med Phys 2019;44:254-62.

For radiation dose measurements, a *p*-type Si diode is more reliable compared to an *n*-type diode.[3,16] Its active volume or die is covered with material both for protection and to provide buildup.[9] *In vivo* measurements with diodes can be made on the patient's surface, in body cavities, or behind the patient.[12,17] Although adequate buildup prevents contaminant electron dose in combination with its intrinsic dose per pulse dependence,[18,19] the use of an IVD diode can perturb patient dose due to its buildup layer thickness.[5,20]

Previous diode-induced dose perturbation studies in megavolt photon beams have employed phantom geometries (such as water tanks or plastic slabs), which differ significantly from patient geometry.[4,5,11,20,21] Some researchers did Kodak X-Omat-V film dosimetry in a polystyrene phantom for an Isorad *p*-type diode.[10] They reported dose reductions ranging from 12% to 30% for photon beams between 4 MV and 18 MV. Under the same measuring conditions, Yaparpalvi *et al*. reported dose reductions of 16% for a 3 cm circular 6 MeV electron field.[20] Sen *et al*. reported beam attenuations of up to 10% along the central axis (CAX) for 6 MV and 10 MV photon beams, and electron beam dose reductions of up to 25% for 6 MeV electron beams for Isorad diodes.[5] Alecu *et al*. studied the dose perturbations in a scanning water phantom with three types of Sun Nuclear Isorad *p*-type diode detectors and found perturbations of up to 13%.[4]

The aim of this study is to investigate the megavoltage photon beam perturbations induced by an *in vivo* diode detector in combination with prosthesis involvement in a realistic pelvic phantom that contains a titanium implant (the prosthesis), water-equivalent soft tissue, and chemically accurate bony structures. Gafchromic film measurements were performed to address the aim.

## Materials and Methods

An IBA Dosimetry EDP-20$^{3G}$ diode detector designed and calibrated for photon IVD in the megavolt photon energy range was used to study its dose shadowing effects and prosthesis involvement on its response. This *p*-type diode has a 2.3-mm stainless steel/2.0-mm epoxy resin buildup that is equivalent to 20 mm of water. Photon beams with nominal energies of 6 MV and 10 MV produced by an Elekta synergy linear accelerator were used to measure the dose perturbations induced by the *in vivo* diode on photon beam dose distributions using Gafchromic EBT3 film pieces in a human-like pelvic phantom. The heterogeneous symmetrical phantom that was developed by 3D printing technology is specially designed for film dosimetry, and it consists of stacked 25 water-equivalent Nylon-12 layers equipped with unilateral hip Ti prosthesis, and the bony structures of the pelvic region and lower abdomen as shown in Figure 1. A thorough description of the phantom including its water equivalence is described elsewhere.[22]

A single calibrated batch of 35.6 cm × 43.2 cm Gafchromic EBT3 film (Lot #:05181601) was used to measure the dose perturbations caused by the EDP-20$^{3G}$ *in vivo* diode. Due to

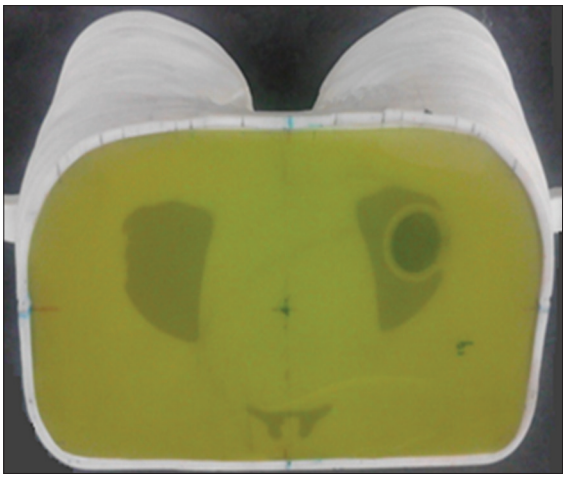

**Figure 1:** The human-like prosthesis phantom oriented in the supine position with inserted Gafchromic EBT3 film piece for measurements (film is in direct contact with the prosthesis). When the phantom is placed in the upright position, the measurement plane is at a depth of 11 cm from the top of the phantom

the relatively weak energy dependence of Gafchromic EBT3 films over a broad range of beam qualities and modalities used clinically in the megavoltage photon and electron energy range, film calibrations were performed in a 10 MV beam in a similar procedure as reported by Ade and du Plessis.[22] A rational function of the type:

$$X(D) = A + \left[B / (D - C)\right] \quad (1)$$

was used where *X (D)* is the optical density (OD) at dose *D* and *A, B,* and *C* are fitting parameters. For the calibration, five 10 cm × 4 cm pieces of film were cut from a single sheet with a small cut marked on each piece to indicate the orientation of the original sheet. The five pieces of film were irradiated inside a 30 cm × 30 cm RW3 slab phantom to various dose values between 0 and 700 cGy. The sequence of monitor units (MUs) set was 0, 200, 400, 800, and 960. Film pieces were placed at 10 cm depth inside the phantom on the CAX of a 10 cm × 10 cm 10 MV photon radiation field at 100 cm source-to-phantom-surface distance (SSD) and irradiated perpendicularly to the 10 MV beam. The film pieces were scanned 24-h post exposure to allow for polymerization.

Films were digitized with an Epson Perfection V330 Photo flatbed document scanner with a resolution of 50 dots per inch (dpi). Each film piece was centered on the scanner bed at 90° before multiple scans of it were taken successively to obtain mean pixel values over an invariant (region of interest = 3 cm × 3 cm) in its center. This avoided OD measurement artifacts near film edges. The process was repeated for all film pieces. Film images were scanned as raw 48-bit RGB (16 bits per color channel) and saved as Tagged Image –File Format (TIFF) image files. The scanned images were processed using the 16 bits red channel. The delivered dose *D* versus measured OD (determined from pixel readings) was then fitted employing the analytical function

depicted in Equation (1). The coefficients *A*, *B,* and *C* were determined utilizing a least-square optimization method and a goodness-of-fit R-squared value of 0.9997 (99.97%) was computed.

For film dose measurements in the prosthesis phantom, the phantom was oriented in the supine position [Figures 1 and 2] with film inserted in the measurement plane and in direct contact with the prosthesis as shown in Figure 1. The measurement orientation was along the axial slices of the phantom with the prosthesis located at 8.5 cm depth from the surface. The measurements commenced as follows as indicated in Figures 2 and 3: first, CAX film dose measurements for 6 MV and 10 MV photon beams were acquired for single antero-posterior (AP) fields between 2 × 2 and 15 cm × 15 cm at a SSD of 91.5 cm. These were done on the side of the phantom with the Ti prosthesis (prosthetic field) and were repeated on the side without the prosthesis (non-prosthetic field). Second, the above measurements were repeated with diode placed on the surface of the phantom along the CAX of the radiation fields to assess its shadowing effect, particularly for prosthetic involvement. 300 MUs were setup for each field delivered at 100 cm source-to-axis distance placed on the prosthesis, and bone for prosthetic and non-prosthetic fields, respectively.

The effect of 10 MV multiple photon beams that include lateral opposing fields and a four-field box plan were also measured with Gafchromic EBT3 film for the diode and prosthesis involvement for configurations as outlined in Figure 3. The position of film in the measurement plane for each multibeam setup shown in Figure 3 is as indicated in Figure 1. As in the measurement utilizing single beam setups, film dose measurements were done with and without the diodes included in the photon fields. The multibeam plans were generated on an Elekta Monaco treatment planning system (TPS) in a computed tomography model of the pelvic phantom. The target dose was set at 500 cGy for a single fraction. Lateral fields were studied since the treatment of prostate may involve the use of lateral fields when two-dimensional conventional or 3D conformal planning is considered.[23] IMRT for prostate cancer may also utilize treatment fields that are lateral or close to lateral.[24,25] The generated treatment plans were then delivered on the Elekta Synergy linac. The phantom was set up with the target positioned at isocenter. The conventional multibeam treatment scenarios comprising the two-field and four-field plans considered in this study were chosen since it is challenging to perform diode dosimetry for modern RT treatment modalities such as VMAT and IMRT. That is, point dose IVD with diodes is not suitable for verifying IMRT and arc-therapy treatments. Diode measurement positions for the conventional multibeam plans are shown in Figure 3.

Irradiated films were scanned after 24 h at a resolution of 50 dpi on the Epson Perfection V330 Photo flatbed document scanner. The scanning orientation of both calibration and measurement films was kept constant by aligning the long axis of the scanner parallel to the long axis of the film. That is, with each film centered on the scanner bed, the film was oriented with its shorter dimension perpendicular to the scanning direction. Landscape orientation (90°) was chosen since it minimizes film orientation effects and the effect of lateral response artifacts on CCD scanners compared to portrait orientation (0°). The resulting images were digitized as raw 48-bit RGB [red green blue] (16 bits per color channel) and stored in TIFF. The 16-bit depth red channel values were used in subsequent dosimetry analysis. Measured dose distributions were analyzed by calculating the percentage discrepancies between film dose data obtained in prosthetic and non-prosthetic fields with and without the *in vivo* diode included in the photon fields. Relative differences were then examined to assess the influence of the Ti prosthesis on the diode-induced photon beam perturbations inside the pelvic phantom.

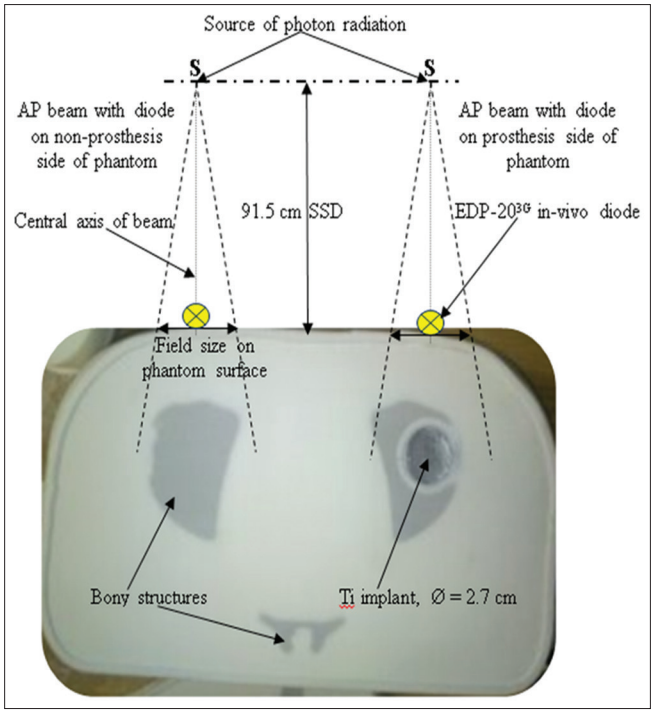


**Figure 2:** Single AP beam setups in the phantom slice for 6 MV and 10 MV photon beam dose distribution measurements with and without an EDP-20[3G] *in vivo* diode placed on the beam's central axis

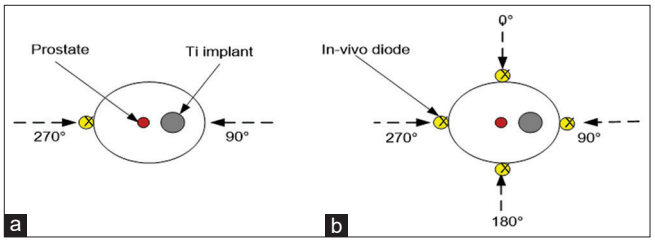


**Figure 3:** Multi-beam setups for a 10 MV photon beam including lateral opposing fields (a) and four-field box (b) plan. The Ti prosthesis and region of interest representing the prostate are also indicated. Film was inserted in the measurement plane and placed over and in direct contact with the prosthesis as indicated in Figure 1

# Results

## Effect of prosthetic fields relative to non-prosthetic fields on diode-induced dose shadow

In the dose range from 145 to 700 cGy, the sensitivity (in terms of net OD per unit absorbed dose) of the studied EBT3 film decreased from 0.003 to 0.001 $cGy^{-1}$.

Figures 4a and b and 5a and b show CAX dose distributions for 6 MV and 10 MV beams measured in the pelvic prosthesis phantom. In Figure 4a and b, film depth dose curves acquired on the prosthesis and non-prosthesis sides of the phantom, respectively, and plots for the ratio of film dose without the diode to film dose when using it are shown for a 5 cm × 5 cm 6 MV field. In Figure 5a and b, 10 MV multibeam film dose data acquired in the phantom for the two-field and four-field techniques, respectively, are shown as well as the differences between dose data measured with and without the diode in the photon fields. In all the figures [Figures 4a - 5b], regions consisting of nylon, bone, and prosthesis indicate where photon beams traverse when incident on the inhomogeneous phantom. The figures show that CAX dose distributions taken with the presence of the *in vivo* diode in the photon fields show dose reductions in the shadow of the diode compared to dose data attained without the diode.

Listed in Tables 1 and 2 are the photon beam dose attenuations quantified as percentages for all the studied single- and multi-field beam setups, respectively, obtained in the human-like prosthesis phantom due to the shadowing effect of the EDP-20[3G] *in vivo* diode and prosthesis involvement on the 6 MV and 10 MV photon beam dose distributions. The presented values represent photon beam attenuations or dose reductions in regions of interest in the distal region of the prosthesis where a lesion is usually located for the treatment of deep-seated pelvic tumors with megavoltage photon beams. The attenuation values for the single-field beam setups presented in Table 1 are specified at a depth of 10 cm, and the dose reductions for the multibeam arrangements tabulated in Table 2 are averaged over depth in the defined target region from 5 cm to 5 cm, which represents a depth range from 10 cm to 20 cm. Both Tables 1 and 2 show dose attenuations acquired on the prosthesis and non-prosthesis sides of the symmetrical pelvic phantom. The uncertainty in the data is within 1% (evaluated as the standard deviation of the average values of three different measurements).

To assess the influence of the prosthesis on the diode-induced dose shadow for single-beam setups, the following situations were considered: the ratios of film depth dose data for (1) a

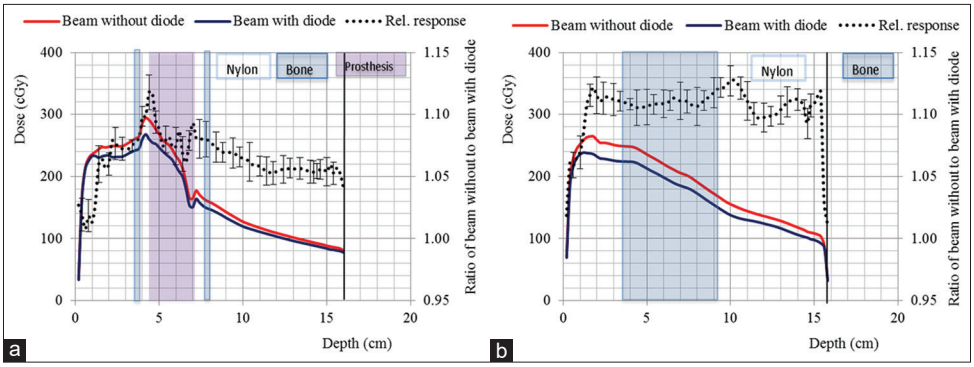


**Figure 4:** (a and b) Depth dose data acquired in the human-like pelvic phantom for a 5 cm × 5 cm 6 MV photon beam. Data are shown for (a) prosthetic (with prosthesis), and (b) non-prosthetic (without prosthesis) fields, with and without the EDP-20[3G] *in vivo* diode on the beam's central axis. Also shown are plots for the ratio of film dose without the diode to film dose when using it. The error bars indicate the random fluctuations of the dose ratios due to radiation scatter and measurement uncertainties

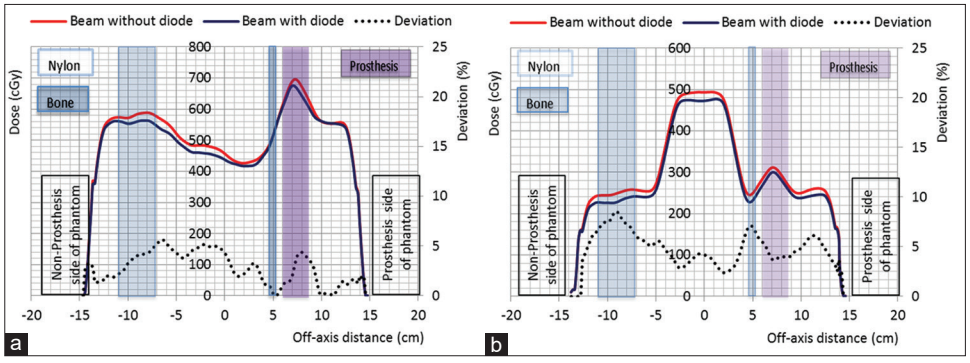


**Figure 5:** (a and b) A comparison of 10 MV photon beam dose distributions acquired in the pelvic prosthesis phantom with and without an EDP-20[3G] *in vivo* diode on the beam's central axis. Also shown are plots for discrepancies between dose data obtained without the diode and when using the diode. Data are shown for lateral opposing fields (a) and four-field box (b) treatment plans. Beam setups for these multifield plans including the positions of the diode on the phantom are indicated in Figure 3

non-prosthetic field with diode to same field without diode and (2) a prosthetic field with diode to same field without diode were calculated. Then, relative differences between the relative responses (defined as the ratio of dose data for a prosthetic [or non-prosthetic] field with diode to same field without diode) of prosthetic and non-prosthetic field data were calculated, as shown in Figure 6a and b, for a 5 cm × 5 cm 6 MV and a 15 cm × 15 cm 10 MV beam, respectively. The calculated relative differences between the dose data in prosthetic and non-prosthetic fields for all single fields are listed in Table 3.

### Effect of prosthetic fields relative to non-prosthetic fields on transmitted diode photons

Tabulated in Table 4 are $d_{50}$ depths (the depth at which the absorbed dose falls to half or 50% of its maximum value) for 6 MV and 10 MV beams for the studied single radiation fields ranging from 2 cm × 2 cm to 15 cm × 15 cm. It is observed for both beam energies that deeper $d_{50}$ depths of 11.5–15 cm are obtained in the non-prosthetic fields compared to shallower $d_{50}$ depths of 8.7–11.5 cm measured in prosthetic fields. This observation is ascribed to the greater attenuation effect of the higher density implant on the prosthesis side of the phantom compared to the bone inhomogeneity on the nonprosthesis side. Table 5 shows relative differences between the $d_{50}$ depths measured in prosthetic and non-prosthetic fields inside the heterogeneous pelvic phantom, illustrating the dosimetric impact of the Ti prosthesis on the photon radiation transmitted through the EDP-20$^{3G}$ *in vivo* diode detector.

**Table 1: The extent of dose shadow (percentage) underneath the EDP-20$^{3G}$ *in vivo* diode on 6 MV and 10 MV photon beam dose distributions measured in a human-like pelvic phantom in prosthetic (with Ti prosthesis) and non-prosthetic (without Ti prosthesis) fields**

| Field size (cm$^2$) | Nonprosthesis side of phantom (%) | | Prosthesis side of phantom (%) | |
|---|---|---|---|---|
| | 6 MV | 10 MV | 6 MV | 10 MV |
| 15×15 | - | 5 | - | 2 |
| 10×10 | 8 | 6 | 6 | 5 |
| 5×5 | 12 | 7 | 7 | 6 |
| 2×2 | 8 | 7 | 7 | 6 |

The percentages are the mean deviations (at a depth of 10 cm in the distal region of the prosthesis where a lesion is usually located for treatments with high-energy photons) between film dose data acquired along the CAX of the beams with and without the *in vivo* diode in the photon fields. The uncertainty in the data is within 1% (evaluated as the standard deviation of the average values of three different measurements). CAX: Central axis

**Table 2: Magnitude of dose shadow (percentage) beneath the EDP-20$^{3G}$ *in vivo* diode on 10 MV multi-beam dose distributions measured in a pelvic prosthesis phantom**

| Multi-beam plan | Dose shadow in phantom on the (%) | | Dose shadow at the target region (%) |
|---|---|---|---|
| | Nonprosthesis side | Prosthesis side | |
| Four-field box | 5 | 4 | 4 |
| Lateral opposing fields | 4 | 2 | 3 |

The percentage values are the mean deviations (averaged over depth on the prosthesis and non-prosthesis sides of the phantom as well as in the target region) between film dose data acquired along the CAX of the beams with and without the diode in the photon fields. CAX: Central axis

## Discussion

Monitoring of patient treatment dose, previously calculated by TPSs, is of paramount importance in radiotherapy. Si diode detectors have traditionally been used for IVD applications

**Table 3: Relative differences (percentage) between dose shadows as found in the beam with and without the Ti prosthesis**

| Field size (cm$^2$) | 6 MV beam (%) | 10 MV beam (%) |
|---|---|---|
| 15×15 | - | 3 |
| 10×10 | 3 | 2 |
| 5×5 | 4 | 2 |
| 2×2 | 3 | 2 |

The percentage values are mean differences between photon beam dose data determined in the human-like pelvic phantom in prosthetic and non-prosthetic fields, averaged over depth (in the distal region of the prosthesis where a lesion is usually located for treatment with MV photon beams), and along the CAX of the photon beams. The uncertainty in the data is within 1% (evaluated as the SD of the average values of three different measurements). SD: Standard deviation, CAX: Central axis

**Table 4: Depths of 50% dose, $d_{50}$ (cm) for 6 MV and 10 MV photon beam depth dose curves determined in a heterogeneous pelvic phantom in prosthetic (with prosthesis) and non-prosthetic (without prosthesis) fields illustrating the influence of the Ti implant on the photon radiation transmitted through the EDP-20$^{3G}$ *in vivo* diode detector for various regular fields**

| Field size (cm$^2$) | $d_{50}$ depths (cm) for non-prosthetic fields with and without EDP diode on CAX | | $d_{50}$ depths (cm) for prosthetic fields with and without EDP diode on CAX | |
|---|---|---|---|---|
| | Without diode | With diode | Without diode | With diode |
| 10 MV fields | | | | |
| 2×2 | 14.2 | 14.8 | 8.7 | 8.8 |
| 5×5 | 13.7 | 14.0 | 8.8 | 8.8 |
| 10×10 | 15.0 | 15.0 | 8.9 | 9.1 |
| 15×15 | 14.4 | 14.8 | 11.5 | 11.4 |
| 6 MV fields | | | | |
| 2×2 | 11.5 | 12.2 | 9.2 | 9.1 |
| 5×5 | 12.7 | 12.8 | 8.7 | 8.9 |
| 10×10 | 14.3 | 14.4 | 9.2 | 9.5 |

The data show shallower $d_{50}$ depths measured in prosthetic fields due to radiation attenuation by the high-density prosthesis compared to the deeper depths for the non-prosthetic fields. CAX: Central axis

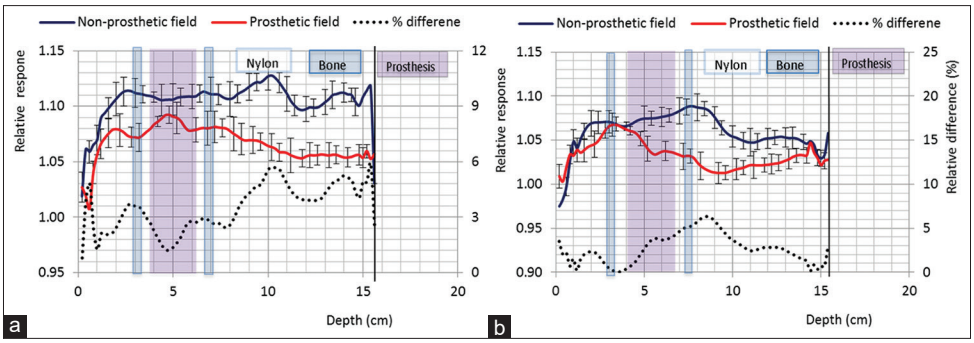


**Figure 6:** Relative response values (ratio of film dose without the EDP-20$^{3G}$ *in vivo* diode to film dose when using the diode) for prosthetic and non-prosthetic (without prosthesis) fields. Also shown are plots for relative differences between the prosthetic and non-prosthetic field data. Data are shown for: (a) a 5 cm × 5 cm 6 MV beam; and (b) a 15 cm × 15 cm 10 MV beam. The error bars indicate the random fluctuations of the dose ratios due to radiation scatter and measurement uncertainties

**Table 5: Relative differences (percentage) between $d_{50}$ depths measured in prosthetic (with prosthesis) and non-prosthetic (without prosthesis) fields inside a heterogeneous pelvic phantom illustrating the influence of the Ti prosthesis on the photon radiation transmitted through the EDP-20$^{3G}$ *in vivo* diode detector**

| Field size (cm$^2$) | Ratios of $d_{50}$ depths with and without *in vivo* diode included in photon beams for prosthetic and non-prosthetic fields | | Relative differences between prosthetic and non-prosthetic fields (%) |
|---|---|---|---|
| | Non-prosthetic fields | Prosthetic fields | |
| 10 MV fields | | | |
| 2×2 | 1.0423 | 1.0115 | 3 |
| 5×5 | 1.0219 | 1.0000 | 2 |
| 10×10 | 1.0000 | 1.0025 | 2 |
| 15×15 | 1.0278 | 1.0088 | 2 |
| 6 MV fields | | | |
| 2×2 | 1.0609 | 1.0110 | 5 |
| 5×5 | 1.0079 | 1.0230 | 2 |
| 10×10 | 1.0070 | 1.0326 | 3 |

The percentage differences were calculated from the ratios of $d_{50}$ depths with and without the *in vivo* diode included in the photon beams for prosthetic and non-prosthetic fields. Data are shown for 6 MV and 10 MV photon beams for various field sizes

to perform a final check of the actual radiation dose given to an individual patient at the patient level. Mindful that *in vivo* diodes are likely to remain the mainstay of simple palliative care treatment even in the advent of EPID-based dosimetry,[14] and that the presence of *in vivo* diodes and metallic interfaces in high-energy radiation fields could perturb the patient radiation dose, this study employed a representative human-like pelvic phantom that contains unilateral Ti prosthesis and bony structures to investigate 6 MV and 10 MV photon beam dose perturbations caused by an EDP-20$^{3G}$ *in vivo* diode in combination with prosthesis involvement for single- and multi-beam setups.

For the studied 2 cm × 2 cm–15 cm × 15 cm single fields [Figure 4a and b and Table 1], the study shows that in the distal region of the prosthesis where a lesion is usually located for treatment with megavoltage photon beams: (1) greater attenuation of a lower-energy photon radiation caused deeper dose shadows acquired for the 6 MV beam compared to shallower values attained for the higher 10 MV beam; (2) although one may expect deeper dose shadows in prosthetic fields compared to non-prosthetic fields due to the higher attenuation effect of the Ti prosthesis compared to bone, the dose attenuations obtained on the prosthesis side of the phantom are lower than those attained on the nonprosthesis side. Such an observation is probably due to the forward scatter dose effect on the exit side (distal interface) of the prosthesis,[26] which tends to lower or compensate for the dose shadow beneath the diode. Being an interface effect, the forward scatter dose is influenced by secondary electrons released from the Ti prosthesis due to photon interaction processes including Compton and pair production. As Figure 4a shows, there is a rapid increase in dose (dose enhancement) at the distal interface of the prosthesis due to the effect of secondary electron transport across the interface. The enhanced dose then tends to counteract the dose shadow underneath the diode; (3) Figure 4a and b also show that the backscatter dose at the proximal nylon-prosthesis interface in reduced when using a diode in the photon fields compared to the case without a diode. This could be attributed to the attenuation effect of the diode which reduces the primary photon radiation reaching the interface before being backscattered, as it was observed in our previous study that the backscatter dose increased with increase in photon energy;[22] (4) the attenuation

effect of the *in vivo* diode and prosthesis involvement shows a small dependence on field size where the dose shadow increases with decreasing field size except for the 6 MV beam for non-prosthetic fields where the dose attenuation increases from a 10 cm × 10 cm field to a 5 cm × 5 cm field, and then decreases again for a 2 cm × 2 cm field.

The field-size dependence of diodes has been observed to vary among different commercial diode detectors, and for diodes with insufficiently thick buildup, electron contamination is a contributing factor.[27] For a Sun Nuclear Isorad photon diode (with a supplemental brass buildup cylinder of 0.965 g/cm$^2$ in thickness and a total buildup thickness of 1.534 g/cm$^2$) positioned on the CAX of a 6 MV photon beam, Sen *et al*. reported slight changes in attenuation from 10.1% for a 4 cm × 4 cm field to 9.2% for a 20 cm × 20 cm field size averaged over the depth from $d_{max}$ to 20 cm.[5] Likewise, Alecu *et al*. reported for a 15 MV beam that the attenuation effect of a Sun Nuclear Isorad photon diode changed from 13.4% for a 5 cm × 5 cm field to 11.6% for a 40 cm × 40 cm field.[4] The slightly higher attenuation effect for smaller fields is attributed to less scatter due to a smaller volume irradiated.[4] A larger field size with more radiation scatter will compensate to some extent for the attenuation of the diode. Table 1 of this study shows that the smallest dose shadow is obtained for the 15 cm × 15 cm 10 MV prosthetic field, which is the largest field studied.

Similar to the results listed in Table 1, the data presented in Table 2 for the 10 MV treatment plans also demonstrate that the dose attenuations measured on the prosthesis side of the phantom are lower than those attained on the non-prosthesis side. Since for IVD an entrance dose measurement at one or more fields would provide an accurate means of checking the prescribed dose delivery to the patient,[1] the data presented in Table 2 show the attenuation effect of the *in vivo* diode and prosthesis involvement measured for one treatment field for the lateral opposing fields technique and all treatment fields for the four-field box plan for a single fraction dose of 500 cGy. The results show that for a given 3D conformal RT procedure such as the four-field box technique employing *N* fractionated photon treatments, the target dose would be reduced by approximately 4% at the end of treatment if *in vivo* measurements are performed more frequently using the EDP-20$^{3G}$ diode for every treatment field,[26,28] and/or for very short courses of fractionated treatments. For instance, the treatment of prostate cancer using hypofractionated radiotherapy is an emerging form of external beam radiotherapy which is an attractive option for low-risk patients who might not be candidates for brachytherapy or who find a 7–8-week course of daily conventional treatment (fractionated doses of 1.8–2 Gy daily fractions) prohibitive because of logistics or costs.[29-31]

Hypofractionated treatment regimens usually deliver radiation doses ranging from 3.5 to 15 Gy per fraction in ≤5 daily fractions.[30,31] Furthermore, a common and relevant use of IVD with diodes is the control or monitoring of total body irradiation (TBI) which requires detectors at the entrance and exit ports of the irradiation.[28,32,33] TBI with external megavoltage photon beams may use parallel-opposed AP/PA or lateral fields. One important task of IVD, in this case, is to determine the dose at the dose specification point, usually taken at mid-pelvis or mid-abdomen.[33] TBI provides a uniform dose of radiation to the whole body, and it can be used to destroy cancerous cells anywhere in the body including solid tumors.[32] Low-dose TBI uses doses of 2–8 Gy given in one to four fractions, and it is known that fractionated TBI leads to a higher incidence of graft rejection compared to the same dose delivered in one fraction.[32]

Presented in Table 6 are various dose perturbation data due to *in vivo* diodes reported in literature for various phantom geometries, dosimetric systems, and photon energies compared to the present study. It is seen that Sen *et al*.[5] measured average attenuations between 7.5% (for a 10 MV beam) and 10% (for a 6 MV beam) compared with the values of 2%–12% reported in this study for the same beam energies though different diode models.

A photon beam depth dose curve basically consists of two regions – the dose buildup region from the phantom surface to the point of maximum dose $D_{max}$ and the exponential decline region beyond $D_{max}$. Several important points or features can be located on the depth dose curve, for instance: the depth of dose maximum $d_{max}$; the depth of 80% dose $d_{80}$; and the depth of 50% dose $d_{50}$. Neglecting the effects of scattering and inverse square law, the variation of absorbed dose with depth $d$ beyond $D_{max}$ could be approximated by exponential attenuation $e^{-<\mu>(d-dmax)}$ where $<\mu>$ is the average attenuation coefficient for the heterogeneous beam (and the medium in which measurement of absorbed dose is made) which takes into account the effect of beam quality.[34] As relative attenuation can be checked by comparing depths at certain percentage of absorbed dose rather than using doses at certain depths,[35] this study compares the depths of 50% dose for measurements made in the pelvic prosthesis phantom for prosthetic and non-prosthetic fields with and without the EDP-20$^{3G}$ diode included in the photon beams so as to evaluate the influence of the Ti implant relative to bony structures on the photon radiation transmitted through the diode. The results, as listed in Tables 4 and 5, show that relative differences ranging from 2% to 5% were obtained between prosthetic and non-prosthetic fields, with lower $d_{50}$ depths were measured for prosthetic fields. Depth dose measurements with and without the diode placed on the CAX of a 10 cm × 10 cm 10 MV field were also made for a simplified homogeneous RW3 plastic slab phantom. Deeper $d_{50}$ depths of 17 cm and 16.1 cm were measured in the homogeneous phantom with and without the diode placed in the beam, respectively, compared to the shallower depths determined in the heterogeneous pelvic phantom [Table 4] for the same 10 cm × 10 cm 10 MV field. The results of this study therefore show that: (1) various beam parameters like the $d_{50}$ depths would vary when measurements are performed using a simplified homogeneous phantom and a realistic heterogeneous phantom and (2) the $d_{50}$ depths are higher with diode placed on the surface of the phantom along the CAX of the beam than without diode due to a reduction of $D_{max}$ as well as $D_{50}$ by the diode, thus pushing $d_{50}$ deeper into the phantom.

**Table 6: Photon dose perturbations due to *in vivo* diodes reported in literature for various photon energies compared to the findings of the present study**

| References and diode types | Photon energy range (MV) | Phantom and dosimetry system | Dose perturbations (%) |
|---|---|---|---|
| Sen *et al*. (1996) Sun Nuclear Isorad diodes | 6-10 | Welhofer water scanning system 0.147 $cm^3$ ion chamber | 7.5-10 |
| Alecu *et al*. (1997) Sun Nuclear Isorad *p*-type diodes | 4-15 | Scanning water phantom 0.1 $cm^3$ ion chamber | 4-13 |
| Colussi *et al*. (2001) Isorad *p*-type diodes | 4-18 | Polystyrene slab phantom Kodak X-Omat-V film | 12-30 |
| This study (2019) IBA EDP-$20^{3G}$ *p*-type diode | 6-10 | Human-like Nylon pelvic phantom Gafchromic EBT3 film | 2-12 |

IBA: Ion beam applications S.A., EBT: External beam therapy

IVD measurements with diodes may be performed for a few treatment sessions and after every change in the treatment procedure,[9,13] and it is uncommon for some clinics to monitor patient dose on a daily basis for every treatment field for the treatment session.[5,28] An analysis of uncertainties related to radiation treatments has shown that a dosimetric accuracy of 3% is required to yield a 5% accuracy in the dose delivered to the patient.[36-39] Since tumors are generally recognized to have a shallower dose–response effect in comparison with normal tissues, the beam perturbations discussed in this study suggest that to minimize a steep change in tumor response, a dosimetric uncertainty >3% due to the attenuation effect of the *in vivo* diode, and prosthesis involvement would be unacceptable as a small underdose to tumors could yield a decrease in the probability of tumor control.[13] Hence, it is evident from the results and discussion that if very short courses of radiation treatments including single fractionated treatment fields are used in the pelvic region as has been reported in a recent study,[40] patient dose reduction due to the shielding effect of the diode and prosthesis involvement would be >3%. As the CAX of the primary treatment beam usually passes through the center of the gross tumor volume, an *in vivo* diode (which is usually placed on the CAX of the treatment beam onto the patient's skin for entrance surface dose measurements) would reduce the dose in a part of the planning target volume where the highest malignant cell concentration may be expected.[4] Hence, patients unintentionally receiving a lower, than the intended dose to the target volume may have an increased risk of local failure.

Although entrance surface dosimetry is the most commonly used geometry for conventional IVD with diode detectors, various possibilities can be adopted to reduce the perturbation effect induced by entrance diodes during IVD, such as by varying the position of the diode over the treatment field or by replacing entrance with exit dose measurements.[4] The former approach could be beneficial to critical structures if the diode is directly positioned above such structures. Hence, the shadowing effect of an *in vivo* diode and prosthesis involvement could have a negative impact on treatment outcome on the one hand if the diode and prosthesis drastically shadow part of a tumor, and a positive effect on the other hand if either or both shield a critical structure in cases where the position of the detector is not varied over the treatment field.

The limitation of this study is that compared to simplified flat phantom measurements which might provide additional data on the impact of an *in vivo* diode on the surface dose, the setup of films in the pelvic phantom does not allow one to get useful information on the surface dose at depths <5 mm in the phantom due to its design. As Figure 4a shows, the surface dose is far below 100%. On the other hand, an advantage of the pelvic phantom is that for studies involving highly-dense inhomogeneities, including metallic interfaces and bony structures, it represents realistic clinical conditions better than simplified homogeneous phantom slabs.

## Conclusion

IVD, during a few treatment sessions, are recommended for some patient groups where a high accuracy in dose delivery is required.[13] *In vivo* measurements with diode detectors represent one of the most important procedures, especially in complex techniques like TBI prior to bone marrow transplantation or other situations with high risk for critical structures such as the bladder and rectum during prostate irradiation. Noting that: (1) fractionated TBI leads to a higher incidence of graft rejection compared to the same dose delivered in one fraction[32] and (2) the guaranty of delivering the appropriate dose in the target volume is essential for good treatment outcome; it is vital to quantify the beam perturbations produced by detectors used during IVD under various realistic conditions.

This study has investigated the beam perturbations induced by an EDP-$20^{3G}$ *in vivo* diode in combination with prosthesis involvement on 6 MV and 10 MV photon beam dose distributions in a human-like phantom that contains unilateral hip Ti prosthesis. Under the studied conditions using various beam setups, photon dose attenuations ranging from 2% to 7% and from 5% to 12% were determined in the phantom for prosthetic and non-prosthetic fields, respectively, with relative differences between 2% and 4%. In addition, $d_{50}$ depths ranging from 8.7 to 11.5 cm and from 11.5 to 15 cm were measured in the phantom for prosthetic and non-prosthetic fields, respectively, with relative differences between 2% and 5%. On the basis of accuracy requirements in RT noting that a small underdose to tumors could yield a decrease in the probability of tumor control, the diode-induced beam perturbations in combination with prosthesis involvement in the photon

radiation fields may affect RT treatment outcome (especially for hypofractionated or single TBI treatments), as there would be a reduction in tumor dose. This study also shows that the presented heterogeneous human-like phantom would provide beam parameters such as $d_{50}$ depths which are representative of certain realistic clinical conditions due to the presence and attenuation effect of inhomogeneities compared to a simplified homogeneous slab phantom.

## Financial support and sponsorship

This work was supported by the Medical Research Council of South Africa in terms of the MRC's Flagships Awards Project (grant number SAMRC-RFA-UFSP-01-2013/HARD).

## Conflicts of interest

There are no conflicts of interest.

## References

1. Howlett S, Duggan L, Bazley S, Kron T. Selective *in vivo* dosimetry in radiotherapy using P-type semiconductor diodes: A reliable quality assurance procedure. Med Dosim 1999;24:53-6.
2. Oliveira FF, Amaral LL, Costa AM, Netto TG. *In vivo* dosimetry with silicon diodes in total body irradiation. Radiat Phys Chem 2014;95:230-2.
3. Huang K, Bice WS Jr., Hidalgo-Salvatierra O. Characterization of an *in vivo* diode dosimetry system for clinical use. J Appl Clin Med Phys 2003;4:132-42.
4. Alecu R, Feldmeier JJ, Alecu M. Dose perturbations due to *in vivo* dosimetry with diodes. Radiother Oncol 1997;42:289-91.
5. Sen A, Parsai EI, McNeeley SW, Ayyangar KM. Quantitative assessment of beam perturbations caused by silicon diodes used for *in vivo* dosimetry. Int J Radiat Oncol Biol Phys 1996;36:205-11.
6. Petoukhova A, Rüssel I, Nijst-Brouwers J, van Wingerden K, van Egmond J, Jacobs D, *et al. In vivo* dosimetry with MOSFETs and GAFCHROMIC films during electron IORT for accelerated partial breast irradiation. Phys Med 2017;44:26-33.
7. Guidi G, Gottardi G, Ceroni P, Costi T. Review of the results of the *in vivo* dosimetry during total skin electron beam therapy. Rep Pract Oncol Radiother 2014;19:144-50.
8. Allahverdi M, Taghizadeh MR. Achievable accuracy in brain tumors by *in vivo* dosimetry with diode detectors. Iranian J Radiat Res (Print) 2006;3:153-61.
9. American Association of Physicists in Medicine. Diode *in vivo* Dosimetry for Patients Receiving External Beam Radiation Therapy, AAPM Report No. 87. American Association of Physicists in Medicine; 2005.
10. Colussi VC, Beddar AS, Kinsella TJ, Sibata CH. *In vivo* dosimetry using a single diode for megavoltage photon beam radiotherapy: Implementation and response characterization. J Appl Clin Med Phys 2001;2:210-8.
11. Eveling JN, Morgan AM, Pitchford WG. Commissioning a p-type silicon diode for use in clinical electron beams. Med Phys 1999;26:100-7.
12. Essers M, Mijnheer BJ. *In vivo* dosimetry during external photon beam radiotherapy. Int J Radiat Oncol Biol Phys 1999;43:245-59.
13. International Atomic Energy Agency. Accuracy Requirements and Uncertainties in Radiotherapy, IAEA Human Health Series No. 31. Vienna: International Atomic Energy Agency; 2016.
14. MacDougall ND, Graveling M, Hansen VN, Brownsword K, Morgan A. *In vivo* dosimetry in UK external beam radiotherapy: Current and future usage. Br J Radiol 2017;90:20160915.
15. Olaciregui-Ruiz I, Vivas-Maiques B, Kaas J, Perik T, Wittkamper F, Mijnheer B, *et al.* Transit and non-transit 3D EPID dosimetry versus detector arrays for patient specific QA. J Appl Clin Med Phys 2019;20:79-90.
16. Zhu XR. Entrance dose measurements for *in-vivo* diode dosimetry: Comparison of correction factors for two types of commercial silicon diode detectors. J Appl Clin Med Phys 2000;1:100-7.
17. Vial P. *In vivo* dosimetry for IMRT. AIP Conf Proc 2011;1345:165-80.
18. Shi J, Simon WE, Ding L, Saini D Rose S. Effects of buildup thickness and material to diode detector SSD dependence. Med Phys 1999;26:1127.
19. Jornet N, Ribas M, Eudaldo T. *In vivo* dosimetry: Intercomparison between p-type based and n-type based diodes for the 16-25 MV energy range. Med Phys 2000;27:1287-93.
20. Yaparpalvi R, Fontenla DP, Vikram B. Clinical experience with routine diode dosimetry for electron beam radiotherapy. Int J Radiat Oncol Biol Phys 2000;48:1259-65.
21. Marre D, Marinello G. Comparison of p-type commercial electron diodes for *in vivo* dosimetry. Med Phys 2004;31:50-6.
22. Ade N, du Plessis FC. Dose comparison between gafchromic film, xiO, and Monaco treatment planning systems in a novel pelvic phantom that contains a titanium hip prosthesis. J Appl Clin Med Phys 2017;18:162-73.
23. Ding GX, Yu CW. A study on beams passing through hip prosthesis for pelvic radiation treatment. Int J Radiat Oncol Biol Phys 2001;51:1167-75.
24. Fattahi S, Ostapiak OZ. An opposed matched field IMRT technique for prostate cancer patients with bilateral prosthetic hips. J Appl Clin Med Phys 2012;13:3347.
25. Brooks C, Cheung RM, Kudchadker RJ. Intensity-modulated radiation therapy with noncoplanar beams for treatment of prostate cancer in patients with bilateral hip prosthesis-a case study. Med Dosim 2010;35:87-91.
26. Dutreix J, Bernard M. Dosimetry at interfaces for high energy X and gamma rays. Br J Radiol 1966;39:205-10.
27. van Dam J, Marinello G. Methods for *in vivo* Dosimetry in External Radiotherapy. ESTRO Booklet on Physics for Clinical Radiotherapy No. 1. Leuven, Apeldoorn: Garant; 1994.
28. Ismail A, Giraud JY, Lu GN, Sihanath R, Pittet P, Galvan JM, *et al.* Radiotherapy quality assurance by individualized *in vivo* dosimetry: State of the art. Cancer Radiother 2009;13:182-9.
29. Picardi C, Perret I, Miralbell R, Zilli T. Hypofractionated radiotherapy for prostate cancer in the postoperative setting: What is the evidence so far? Cancer Treat Rev 2018;62:91-6.
30. Zaorsky NG, Showalter TN, Ezzell GA, Nguyen PL, Assimos DG, D'Amico AV, *et al.* ACR appropriateness criteria for external beam radiation therapy treatment planning for clinically localized prostate cancer, part II of II. Adv Radiat Oncol 2017;2:437-54.
31. Madsen BL, Hsi RA, Pham HT, Fowler JF, Esagui L, Corman J. Stereotactic hypofractionated accurate radiotherapy of the prostate (SHARP), 33.5 gy in five fractions for localized disease: First clinical trial results. Int J Radiat Oncol Biol Phys 2007;67:1099-105.
32. Wills C, Cherian S, Yousef J, Wang K, Mackley HB. Total body irradiation: A practical review. Appl Radiat Oncol 2016;5:11-7.
33. van Dam J, Marinello G. European Society for Therapeutic Radiology and Oncology: Methods for *in vivo* dosimetry in external radiotherapy, ESTRO Booklet No. 1. 2nd ed. Brussels: ESTRO; 2006.
34. Khan FM. Physics of Radiation Therapy. 3rd ed. USA: Lippincott Williams and Wilkins; 2003.
35. Buzdar SA, Rao MA, Nazir A. An analysis of depth dose characteristics of photon in water. J Ayub Med Coll Abbottabad 2009;21:41-5.
36. International Commission on Radiation Units and Measurements. Determination of Absorbed Dose in a Patient Irradiated by Beams of X or Gamma Rays in Radiotherapy Procedures, Report. 24. Bethesda, MD: International Commission on Radiation Units; 1976.
37. Dutreix A. When and how can we improve precision in radiotherapy? Radiother Oncol 1984;2:275-92.
38. Mijnheer BJ, Battermann JJ, Wambersie A. What degree of accuracy is required and can be achieved in photon and neutron therapy? Radiother Oncol 1987;8:237-52.
39. Mijnheer BJ, Harrison RM. editor. The Clinical Basis for Dosimetric Accuracy in Radiotherapy. United Kingdom: British Institute of Radiology; 1996.
40. McDonald TL, Hung AY, Thomas CR, Wood LJ. Localized external beam radiation therapy (EBRT) to the pelvis induces systemic IL-1Beta and TNF-alpha production: Role of the TNF-alpha signaling in EBRT-induced fatigue. Radiat Res 2016;185:4-12.